Journal of Sound and Vibration (1999) **221**(4), 651–679
Article No. jsvi.1998.2026, available online at http://www.idealibrary.com on IDEAL

A COMPARATIVE STUDY OF METHODS FOR OPTIMISING SENSOR AND ACTUATOR LOCATIONS IN ACTIVE CONTROL APPLICATIONS

P. De Fonseca, P. Sas and H. Van Brussel
Department of Mechanical Engineering, Division of Production Techniques, Machine Design and Automation PMA, Katholieke Universiteit van Leuven, Celestijnenlaan 300B, B-3001 *Heverlee, Belgium*

(*Received* 20 *October* 1997, *and in final form* 21 *October* 1998)

The present study addresses the optimisation of the locations of the error sensors and the control actuators in an active noise and vibration control system. This system is implemented on a double panel partition in order to improve its sound insulation characteristics in the low frequency range. For this purpose, a model of the active control system is first presented and combined with a model of the considered vibro-acoustic system. This yields an integrated simulation model of the actively controlled structure, allowing both structural and acoustical control. Afterwards, the locations of the control actuators and the error sensors are optimised in order to increase the performance of the active noise and vibration control system, defined as the average reduction of the radiated sound power over the frequency band of interest. Different optimisation algorithms have been implemented. Besides the genetic algorithm, which is naturally well-suited for discretised problems, a number of gradient methods are also tested. Finally the performances of all methods are compared in terms of quality of the obtained solution, computation time and algorithm complexity. This comparison shows that the best gradient method converges faster and yields a better final solution than the best genetic algorithm or than the randomly perturbed gradient method.

1. INTRODUCTION

In principle, active noise control can be viewed as the superposition of a secondary sound field, generated by the control system, on a primary, disturbing sound field such that the residual sound field is as small as possible. So, basically, the objective of the active control system is to generate a secondary sound field that matches the primary sound field as closely as possible, both in time and in space. The quality of the temporal match is determined by the control algorithm, while the quality of the spatial match is mainly influenced by the spatial configuration of the control sources and the error sensors.

0022–460X/99/040651 + 29 $30.00/0

As the cost associated with the commercial implementation of such an active control system is still very high, the system should be optimised prior to its actual installation. This optimisation process should focus on both the physical and the electronic part of the active control system. The optimisation of the electronic part deals with all control theory and signal processing problems, and should result in a controller which reaches its control objective (for example the minimisation of the maximum error signal or the minimisation of the sum of the squared error signals) as closely as possible (for a good temporal match). The present paper, however, focuses on the optimisation of the physical part, assuming a control system which perfectly realises the desired control objective. More specifically, the problem of optimising the number and the locations of the error sensors and the control actuators is addressed, because previous studies [1–12] proved that this spatial configuration of sensors and actuators strongly affects the effectiveness of an active control system (due to the required spatial match). This explains the need for a good optimisation routine for choosing the appropriate sensor and actuator number and positions. Several authors have already studied this problem during the past 5 years, using, however, different optimisation approaches.

In the early papers, the conventional gradient-based optimisation routines were most often used to solve the considered problem. Clark and Fuller [1] and Wang *et al*. [2] determined the size and the location of piezoelectric actuators and sensors on a rectangular plate for active structural acoustic control by means of a commercially available constrained optimisation routine. They defined the objective function as the sum of squared sound pressure values in a discrete number of points in the space above the plate and at a single frequency. The gradients of the objective function and the constraints with respect to the design variables were approximated with central finite differences. Yang *et al*. [3] determined simultaneously the locations and the source strengths of the secondary actuators in an active noise control system in an enclosure, such that the acoustic potential energy is minimised. This simultaneous optimisation of locations and control source strengths complicates the problem, as the control source strengths can be directly calculated by means of the traditional quadratic controller model [4] for given error sensor and control source positions. Also they did not consider the problem of positioning the error sensors as they assumed that there were a ''reasonable number'' of microphones uniformly distributed throughout the cavity. Their optimisation procedure is based on a sequential quadratic programming (SQP) algorithm for constrained optimisation problems. The gradients of the objective function and the constraints are again approximated with finite differences, and the objective function is again defined as the sum of squared sound pressures in a number of points. They found that for the simple case of a rigidly walled rectangular enclosure, at a single frequency, the optimal control loudspeaker tends to form a dipole with the primary sound source. Nayroles *et al*. [5] proposed an approximation method for converting a discrete description of the acoustic system under study to a continuous description. They viewed their diffuse approximation method as a replacement for finite element methods, and used it as an estimation tool for the

evaluation of a function and its gradient in an optimisation process of the source positions in an active absorption system. They recognised that the problem of optimising anti-noise source positions is essentially non-convex, even when only a single frequency is considered and abstraction is made of the positioning of the error sensors. They proposed two gradient methods for solving the non-convex unconstrained optimisation problem, however, without making a comparison between the performances of both methods. Benzaria and Martin [6, 7] used the same diffuse approximation method as Nayroles *et al.* [5] to build a continuous description of a numerical vibro-acoustic model of a cavity bounded by a cylindrical shell. In a first study [6] they observed that a simple selection procedure works quite well when the number of possible locations for the control sources is very limited. Later [7] they combined this selection procedure, generating an initial control source arrangement, with the Polak–Ribière unconstrained optimisation algorithm for finding a good actuator configuration in a more complex situation (i.e., with much more feasible positions for the control sources). They concluded that trends exist for the sources to work together as dipoles or quadripoles in certain areas of attraction, which are acting independently on an image of the maxima of the single-tone primary field. Clearly, this kind of observation can be expected to become very difficult when optimising the control source locations for a broadband disturbing field.

So far, all papers have focused on a single-frequency primary field for the optimisation of the active control system configuration. A second tendency in the literature dealing with the optimisation of actuator and sensor positions in an actively controlled system, is based on the work of Burdisso and Fuller [8, 9]. They proved, for the case of a simply supported beam, that the dynamic characteristics of the controlled structure are totally different from those of the original structure, and that the controlled eigenvalues and eigenmodes are functions of both the control actuators and the error sensor locations. Hence, an optimisation process reducing some objective function at only one or a few frequencies, suffers from the severe drawback that the resonances of the controlled system may lie close to one of those frequencies. This leads to a lack of robustness in the optimised controlled system against small frequency variations in the disturbing input. Therefore, the optimisation should always be performed over a certain frequency band, or it should be verified that the eigenfrequencies of the controlled system lie away from the dominant frequencies in the disturbing excitation. The latter requirement is further elaborated in the eigenvalue assignment procedure for designing "optimal" feedforward control systems by Burdisso and Fuller [10] and by Rodriguez *et al.* [11]. They first determined the optimal properties of the control actuators and the error sensors in the modal domain, based on the desired eigenvalues of the controlled system. In a second stage, these sensor and actuator properties in the modal domain have to be translated into physical characteristics and locations. This problem remains very difficult to solve for real-life structures which cannot be modelled analytically and with more than only a few dominating eigenmodes. Burdisso and Fuller [12] developed a similar methodology to design active structural acoustic control systems for minimal sound radiation. However, the problem of

translating the "optimal" sensor and actuator properties in the modal domain to physical properties remains the same. Although the theory on the eigenproperties of actively controlled structures provides a lot of valuable insights into the problem, it does not present a general framework for optimising the sensor and actuator positions on a complex real-life structure.

The third tendency in the literature on sensor and actuator optimisation in an active control system, follows a more pragmatic way. Based on the observation that the radiated sound power or the acoustic potential energy in an enclosure is a strongly non-linear and non-convex function of the positions of the control actuators and the error sensors in an active control system (see for example reference [5]), some people started to look at more global optimisation techniques, mainly genetic algorithms [13, 14], as an alternative to the classical optimisation methods, which are likely to converge to a local optimum. Moreover, genetic algorithms are well-suited for problems where the dynamic behaviour of the considered structure is known only in a few points, for example from measurements. Tsahalis *et al.* [15] applied a genetic algorithm to find the optimal loudspeaker positions for an active noise control system implemented in a propeller aircraft with a pure tone primary excitation. Wang [16] replaced the constrained optimisation routine from a previous study [2] by a genetic algorithm to determine the optimal microphone and piezoelectric actuator configuration on an actively controlled, simply supported beam excited at a single frequency. However, he made no comparison between the performances of the constrained optimisation routine and the genetic algorithm. Hansen *et al.* [17] presented a nice overview of several types of genetic algorithms with their respective advantages and drawbacks for application to the problem of optimising control source locations in an active control system. De Fonseca *et al.* [18] optimised the error microphone and control loudspeaker positions along the border of the cavity in an actively controlled double glazing window by means of a genetic algorithm. Their experimental results show a fairly good qualitative agreement between the predicted and the measured transmission losses. Moreover, the measured performance of an active noise control system in an optimised configuration is much better than that in an intuitively chosen configuration. Baek and Elliot [19] compared genetic algorithms and simulated annealing methods for optimising control source locations in a rectangular enclosure with a pure-tone primary field. They concluded that the performances of both methods on the problem being considered are comparable, but that the genetic algorithms are less sensitive to the tuning of some characteristic parameters than the simulated annealing method. Souza de Cursi and Cortes [20] used the randomly perturbed gradient method [21, 22] to select the optimal secondary source positions along a line in a two-dimensional enclosure. In this method, which resembles simulated annealing in some sense, the step in the gradient direction is supplemented in each direction with a random component of decreasing amplitude. This procedure aims at exploring a large area of the search domain, while still taking into account the local gradient information that pushes the search process much quicker to the optimum than in the case of the usual genetic algorithm. Their simulations show that this randomly perturbed

gradient method finds better solutions than the fixed-step steepest descent method.

The previous discussion illustrates that several approaches to the problem of sensor and actuator position optimisation in an active control system have been explored. To the authors' knowledge, until now no attempt has been made to unify the attainments of these approaches. As a first step in this direction, this paper presents a general simulation environment for the analysis of actively controlled vibro-acoustic systems and for the optimisation of the sensor and actuator configuration. No restrictions are imposed on the type of error sensors or control actuators. As this general simulation environment is based on a finite element description of the considered mechanical systems, its applicability extends to complex vibro-acoustic systems (including of course purely structural or purely acoustical systems), which cannot be modelled analytically anymore. Afterwards, different algorithms for optimising sensor and actuator locations have been implemented and tested. The ultimate goal of an optimisation algorithm in this engineering application is to find a very good control configuration in a limited time. This means that the speed of convergence to a good solution is much more important than a theoretical proof on the convergence properties on an infinite time horizon. The performances of genetic algorithms are compared with those of several classical gradient methods and with those of the randomly perturbed gradient methods. In order to take into account the effect of the new resonances of the controlled system in the optimisation process, the disturbing input is a multi-tone signal, and the objective function is the radiated sound power averaged over the frequency band of interest.

The test set-up used in this study is a double wall structure representing a section of an aircraft fuselage and is described in the next section. The simulation of the dynamic behaviour of the double panel partition and of the control algorithm is discussed in section 3. The combination of both simulation models provides the integrated simulation tool for optimising the sensor and actuator positions. Section 4 clarifies the optimisation problem and defines the objective function. Sections 5 and 6 discuss the application of genetic algorithms and gradient methods, respectively, to the considered optimisation problem. Section 7 compares the performances of the different methods in terms of convergence speed and quality of the obtained sensor and actuator configuration. Finally, some conclusions are drawn in the last section.

2. THE EXPERIMENTAL ARRANGEMENT

The basic test set-up consists of a double wall partition, formed by two plane, parallel aluminium panels, clamped to a 10-mm thick and 100-mm high rectangular steel framework. The free dimensions of the plates are 1460×760 mm. This partition is mounted in the upper opening of a rigidly walled enclosure, which is built in the floor of a semi-anechoic room. A loudspeaker placed in the enclosure under the floor provides the acoustical excitation of the double wall structure. In this way the lower panel represents the

outer fuselage of an aircraft (the skin panel) and the upper panel represents the inner fuselage (the trim panel). The free space above the upper panel may be viewed as the passenger's cabin, while the loudspeaker simulates the propeller excitation of the fuselage. The investigated frequency range is from 20 to 250 Hz.

The fuselage test section has about 50 coupled modes below 250 Hz, so its modal density is comparable to that of many real-life structures. This ensures that the problem of optimising the error sensor and control actuator locations on this test article is difficult enough such that the conclusions drawn in this paper are valid not only for academic test cases, but for a large class of practical problems.

Figure 1 shows the experimental arrangement of the double wall partition being considered. In order to have a representative model of an aircraft fuselage section, the dimensions and spacing of the so-called frames (i.e., the circumferential stiffening of the fuselage) and the stringers (i.e., the axial stiffening of the fuselage) on the skin panel are based on those found in a real aircraft.

3. SIMULATION OF THE DYNAMIC BEHAVIOR OF THE ACTIVELY CONTROLLED DOUBLE PANEL PARTITION

3.1. DYNAMIC BEHAVIOUR OF THE DOUBLE PANEL PARTITION

First, a finite element model of the double wall structure has been built. The model comprises the structural subsystem (the skin panel, the stiffeners and the trim panel), the acoustical subsystem (the cavity between the trim and the skin panel and the rigidly walled enclosure under the skin panel), and the fluid–structure interaction between both subsystems. This fluid–structure interaction

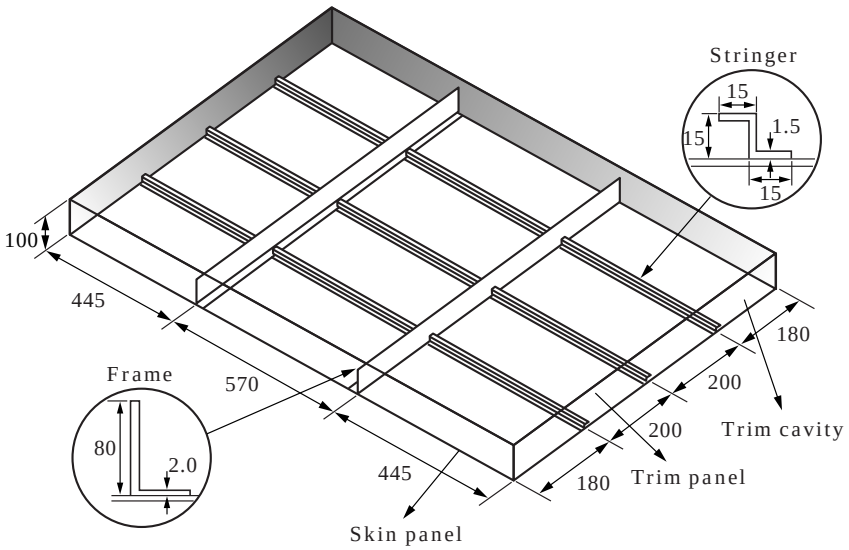

Figure 1. The test set-up.

takes into account the additional loading of the structural subsystem by the presence of the acoustical medium, and the excitation of the acoustical medium by the vibrating structural subsystem. Neglecting damping, the vibro-acoustic system is described by:

$$([\mathbf{K}] - \omega^2[\mathbf{M}])\{\mathbf{X}\} = \left(\begin{bmatrix} [\mathbf{K}_s] & -[\mathbf{K}_c] \\ [\mathbf{0}] & [\mathbf{K}_a] \end{bmatrix} - \omega^2 \begin{bmatrix} [\mathbf{M}_s] & [\mathbf{0}] \\ [\mathbf{M}_c] & [\mathbf{M}_a] \end{bmatrix} \right) \begin{Bmatrix} \mathbf{u} \\ \mathbf{p} \end{Bmatrix} = \begin{Bmatrix} \mathbf{F}_s \\ \mathbf{F}_a \end{Bmatrix}. \quad (1)$$

The column vector of unknowns $\{\mathbf{X}\}$ contains the displacements $\{\mathbf{u}\}$ in the structural nodes and the pressures $\{\mathbf{p}\}$ in the acoustical nodes. $[\mathbf{K}_s]$, $[\mathbf{K}_a]$ and $[\mathbf{M}_s]$, $[\mathbf{M}_a]$ are the structural and acoustical stiffness and mass matrices, while the fluid–structure interaction is modelled in the coupling matrices $[\mathbf{K}_c]$ and $[\mathbf{M}_c]$. As a result of the vibro-acoustic reciprocity [23] principle, the following relation holds between $[\mathbf{K}_c]$ and $[\mathbf{M}_c]$:

$$[\mathbf{M}_c] = \rho[\mathbf{K}_c]^T, \quad (2)$$

where ρ is the density of the acoustic medium.

$\{\mathbf{F}_s\}$ contains the external forces applied to the structural nodes, while the external acoustical excitation vector $\{\mathbf{F}_a\}$ is related to the volume velocity vector $\{\mathbf{Q}\}$ (containing the source strengths of sound sources in the acoustical nodes) by:

$$\{\mathbf{F}_a\} = \rho\{\dot{\mathbf{Q}}\}. \quad (3)$$

As a typical finite element model contains several hundreds or even thousands of nodes, the modal transformation is used to reduce the number of degrees of freedom of the original system:

$$\begin{Bmatrix} \mathbf{u} \\ \mathbf{p} \end{Bmatrix} = \begin{bmatrix} \mathbf{\Phi}_s \\ \mathbf{\Phi}_a \end{bmatrix} \{\mathbf{q}\} = [\mathbf{\Phi}]\{\mathbf{q}\}, \quad (4)$$

in which the columns of the mode shape matrix $[\mathbf{\Phi}]$ contain the right eigenvectors $\{\mathbf{\Phi}_i\}$ of the undamped coupled vibro-acoustic system:

$$([\mathbf{K}] - \omega_i^2[\mathbf{M}])\{\mathbf{\Phi}_i\} = [\mathbf{0}]. \quad (5)$$

The eigenfrequency corresponding to the right eigenvector $\{\mathbf{\Phi}_i\}$ is denoted as ω_i. The eigenvectors consist of two parts, the first being related to the structural subsystem (subscript s) and the second to the acoustical subsystem (subscript a).

Since the coefficient matrices $[\mathbf{K}]$ and $[\mathbf{M}]$ are not symmetrical, the following orthogonality conditions are generally *not* satisfied for coupled systems:

$$\{\mathbf{\Phi}_i\}^H[\mathbf{K}]\{\mathbf{\Phi}_j\} = 0 \quad \text{and} \quad \{\mathbf{\Phi}_i\}^H[\mathbf{M}]\{\mathbf{\Phi}_j\} = 0, \quad \text{for} \quad i \neq j. \quad (6)$$

This non-symmetry of the matrices $[\mathbf{K}]$ and $[\mathbf{M}]$ implies that the right and left eigenvalue problems give different solutions. However, for the special form of non-symmetry (due to the vibro-acoustical reciprocity) of equation (1), it can be proven [24] that the left eigenvectors,$\{\bar{\mathbf{\Phi}}_i\}$, contained in the columns of the matrix$[\bar{\mathbf{\Phi}}]$, are related to the right eigenvectors:

$$\{\bar{\mathbf{\Phi}}_i\} = \begin{Bmatrix} \bar{\mathbf{\Phi}}_{si} \\ \bar{\mathbf{\Phi}}_{ai} \end{Bmatrix} = \begin{Bmatrix} \mathbf{\Phi}_{si} \\ \dfrac{1}{\omega_i^2}\mathbf{\Phi}_{ai} \end{Bmatrix}. \tag{7}$$

The diagonal modal mass and stiffness matrices, [**m**] and [**k**], follow from the left and right multiplication of the original mass and stiffness matrices, [**M**] and [**K**], with the left and right eigenvectors,[$\bar{\mathbf{\Phi}}$]and[$\mathbf{\Phi}$], respectively:

$$[\mathbf{m}] = [\bar{\mathbf{\Phi}}]^H[\mathbf{M}][\mathbf{\Phi}] \quad \text{and} \quad [\mathbf{k}] = [\bar{\mathbf{\Phi}}]^H[\mathbf{K}][\mathbf{\Phi}]. \tag{8, 9}$$

Due to the normalisation of the eigenmodes with respect to the mass matrix, the modal mass matrix equals the unity matrix, and the modal stiffness matrix contains the squares of the natural frequencies ω_i:

$$[\mathbf{k}] = \mathrm{diag}(\omega_i^2). \tag{10}$$

Introducing proportional damping, the modal model becomes:

$$[\mathbf{a}]\{\mathbf{q}\} = ([\mathbf{k}] + \mathrm{j}\omega[\mathbf{c}] - \omega^2[\mathbf{m}])\{\mathbf{q}\} = \{\mathbf{f}\}, \tag{11}$$

where the modal damping matrix is assumed to be diagonal:

$$[\mathbf{c}] = \mathrm{diag}(2\varsigma_i\omega_i), \tag{12}$$

with ς_i the modal damping ratio of the ith coupled mode.

Pre-multiplying the excitation force vector with the left eigenvector matrix yields the modal excitation vector:

$$\{\mathbf{f}\} = [\bar{\mathbf{\Phi}}_s^H \quad \bar{\mathbf{\Phi}}_a^H] \begin{Bmatrix} \mathbf{F}_s \\ \mathbf{F}_a \end{Bmatrix}. \tag{13}$$

For a practical implementation, the numerically calculated mode shapes are compared with those resulting from an experimental modal analysis, and the calculated eigenfrequencies are substituted by the eigenfrequencies of the corresponding experimentally determined mode shapes. Also the modal damping ratios are taken as the result of the experimental modal analysis. This yields a qualitatively reliable simulation model to study the influence of the active control system on the double wall structure.

3.2. SIMPLIFIED CONTROLLER MODEL

The control system consists of a number of control loudspeakers, driven by a control law. In many cases this control law is derived so as to minimise some cost function or performance index. In accordance with other research work dealing with the simulation of the behaviour of active control systems [4, 25–29], the controller objective function in the present study is chosen to be the sum of the squared response signals of a few transducers installed on the structure being

considered. The reason for this choice is that efficient and robust algorithms exist for realising this objective (see for example reference [4]).

Assuming a linear system, the total dynamic response is the superposition of the response to the disturbing excitation and the response to the secondary excitation by the control actuators:

$$\{\mathbf{q}\}_{total} = \{\mathbf{q}\}_p + \{\mathbf{q}\}_c = [\mathbf{a}]^{-1}([\bar{\mathbf{\Phi}}]^H\{\mathbf{F}\}_p + [\bar{\mathbf{\Phi}}(\mathbf{r}_c)]^H\{\mathbf{L}_c\}) \tag{14}$$

The subscript p refers to the primary disturbing excitation, while the subscript c refers to the secondary or control excitation. The vector $\{\mathbf{L}_c\}$ (of dimensions *cx1*) contains the source strength of each of the c control actuators. The matrix $[\bar{\mathbf{\Phi}}(\mathbf{r}_c)]$ (of dimensions *cxm*) describes the modal influence of the control actuators on the considered system. As only point force actuators are considered in this study, its columns contain the left eigenvectors evaluated at the position $\mathbf{r}_{c_i}$ of each control actuator:

$$[\bar{\mathbf{\Phi}}(\mathbf{r}_c)] = \begin{bmatrix} \bar{\mathbf{\Phi}}_1(\mathbf{r}_{c_1}) & \bar{\mathbf{\Phi}}_2(\mathbf{r}_{c_1}) & \cdots & \bar{\mathbf{\Phi}}_m(\mathbf{r}_{c_1}) \\ \cdots & \cdots & & \cdots \\ \bar{\mathbf{\Phi}}_1(\mathbf{r}_{c_c}) & \bar{\mathbf{\Phi}}_2(\mathbf{r}_{c_c}) & \cdots & \bar{\mathbf{\Phi}}_m(\mathbf{r}_{c_c}) \end{bmatrix}. \tag{15}$$

The assumption of point force actuators does not imply any lack of generality of the present approach as the modal influence matrices of other types of actuators (for example distributed piezoelectric actuators) can easily be incorporated into the proposed model.

The controller determines the strengths $\{\mathbf{L}_c\}$ of the control actuators by minimising a cost function Z, which depends on the signals of the error sensors $\{\mathbf{E}\}$. When the control configuration contains e error sensors, the vector of error signals $\{\mathbf{E}\}$ (of dimensions *ex1*) is:

$$\{\mathbf{E}\} = [\mathbf{\Phi}(\mathbf{r}_e)]\{\mathbf{q}\}_{total}. \tag{16}$$

The matrix $[\mathbf{\Phi}(\mathbf{r}_e)]$ (of dimensions *exm*) contains the right eigenvectors evaluated at the position $\mathbf{r}_{e_i}$ of each error sensor:

$$[\mathbf{\Phi}(\mathbf{r}_e)] = \begin{bmatrix} \mathbf{\Phi}_1(\mathbf{r}_{e_1}) & \mathbf{\Phi}_2(\mathbf{r}_{e_1}) & \cdots & \mathbf{\Phi}_m(\mathbf{r}_{e_1}) \\ \cdots & \cdots & & \cdots \\ \mathbf{\Phi}_1(\mathbf{r}_{e_e}) & \mathbf{\Phi}_2(\mathbf{r}_{e_e}) & \cdots & \mathbf{\Phi}_m(\mathbf{r}_{e_e}) \end{bmatrix}. \tag{17}$$

This matrix $[\mathbf{\Phi}(\mathbf{r}_e)]$ also includes some weighting factors to account for differences in amplification between acoustical (e.g., from microphones) and vibration error signals (e.g., from accelerometers or PVDF distributed sensors).

The cost function Z is the sum of the squared error signals. Mathematically the following quadratic minimisation problem has then to be solved:

$$\min Z = \{\mathbf{E}\}^H\{\mathbf{E}\}. \tag{18}$$

Substituting equations (14) and (16) into equation (18) yields:

$$\min Z = (\{\mathbf{F}\}_p^H[\bar{\mathbf{\Phi}}] + \{\mathbf{L}_c\}^H[\bar{\mathbf{\Phi}}(\mathbf{r}_c)])[[\mathbf{a}]^{-1}]^H[\mathbf{\Phi}(\mathbf{r}_e)]^H[\mathbf{\Phi}(\mathbf{r}_e)][\mathbf{a}]^{-1} \times ([\bar{\mathbf{\Phi}}]^H\{\mathbf{F}\}_p + [\bar{\mathbf{\Phi}}(\mathbf{r}_c)]^H\{\mathbf{L}_c\}). \quad (19)$$

The cost function Z reaches its minimum when the derivative to the vector containing the variable secondary source strengths equals zero [4], which produces the resulting $\{\mathbf{L}_c\}$ that minimises Z (superscript + denotes the pseudo-inverse):

$$\{\mathbf{L}_c\} = -[\mathbf{h}]^+[\mathbf{\Phi}(\mathbf{r}_e)][\mathbf{a}]^{-1}[\bar{\mathbf{\Phi}}]^H\{\mathbf{F}\}_p, \quad (20)$$

with

$$[\mathbf{h}] = [\mathbf{\Phi}(\mathbf{r}_e)][\mathbf{a}]^{-1}[\bar{\mathbf{\Phi}}(\mathbf{r}_c)]^H, \quad (21)$$

the matrix of transfer functions between the control inputs and the error sensor responses.

When a vibro-acoustic system is subject to a primary excitation and controlled by a certain control configuration (i.e., with a certain amount of error sensors e and of control actuators c), the resulting response is obtained by combining equations (14) and (20). This response clearly depends on positions of both the error sensors and the control actuators.

4. OPTIMISATION OF SENSOR AND ACTUATOR LOCATIONS

A major objective of this research work is the optimisation of the positions of the error sensors and the control actuators on the skin or the trim panel or in the trim cavity. Positions in the radiated field are not considered as feasible in this study. Instead of using a very time consuming experimental trial-and-error procedure, the optimum control configuration can be determined from the vibro-acoustic model by optimising some objective function. Clearly, the sound energy radiated into the aircraft interior is the most appropriate objective function to minimise. The objective function Π then takes the following form:

$$\Pi = \frac{1}{f_N - f_0}\sum_{f=f_0}^{f_N}\{\dot{\mathbf{u}}_{trim}(f)\}^H[\mathbf{\Sigma}(f)]\{\dot{\mathbf{u}}_{trim}(f)\}, \quad (22)$$

in which f_0 and f_N indicate the first and last frequency line of the frequency band of interest (from 20 to 250 Hz). The radiation impedance matrix of the trim panel $[\mathbf{\Sigma}(f)]$ contains participations of the velocities of the trim panel nodes in the total radiated power, and is calculated using the elemental radiators approach presented by Vitiello *et al.* [30] and by Elliot and Johnson [31]. In general, this matrix $[\mathbf{\Sigma}(f)]$ is non-diagonal and frequency-dependent, as indicated by the notation "(f)". For sake of brevity, this notation will be omitted further on, like in the first part of the paper, as it is clear from the theoretical

background which quantities are frequency-dependent and which are not. Restating equation (22) in terms of modal co-ordinates gives:

$$\Pi = \frac{1}{f_N - f_0} \sum_{f=f_0}^{f_N} \{\mathbf{q}\}^H [\mathbf{M}] \{\mathbf{q}\} (2\pi f)^2, \tag{23}$$

where

$$[\mathbf{M}] = [\mathbf{\Phi}_{trim}]^H [\mathbf{\Sigma}] [\mathbf{\Phi}_{trim}] \tag{24}$$

is the matrix of radiation resistances for the mode shapes of the trim panel in the coupled vibro-acoustic system. This matrix [**M**] can be calculated beforehand for all frequency lines of interest, and stored in the internal memory of the computer during the optimisation process.

The vector {**q**} containing the modal co-ordinates at a certain frequency equals:

$$\{\mathbf{q}\} = [\mathbf{a}]^{-1} ([\mathbf{I}] - [\bar{\mathbf{\Phi}}(\mathbf{r}_c)]^H [\mathbf{h}]^+ [\mathbf{\Phi}(\mathbf{r}_e)] [\mathbf{a}]^{-1}) \{\mathbf{f}\}_p. \tag{25}$$

Because the matrices $[\bar{\mathbf{\Phi}}(\mathbf{r}_c)]$ and $[\mathbf{\Phi}(\mathbf{r}_e)]$ only have a very limited number of rows, as there are only relatively few actuators and sensors in the control system (compared to the total number of degrees of freedom in the model), the expensive multiplication of large matrices can be avoided in a practical implementation, resulting in acceptable computation times for the optimisation routine (about 30 s on a modern workstation).

The radiated sound power is a strongly non-convex function of the error sensor and control actuator locations. This was already recognised by several authors ([5, 19, 20]), and is illustrated for this study in Figure 2. This figure shows the reduction of the radiated sound power with an active control system with four error sensors on the trim panel and two control loudspeakers in the trim cavity. One loudspeaker position is fixed in (0·28, 0·28), while the position of the second one varies over the mid-plane of the cavity. The objective function has a local optimum when both loudspeakers are close to each other, but the global optimum occurs for the second loudspeaker near position (1·2, 0·4).

It is also worthwhile to notice that the definition of the objective function (22) involves a broadband optimisation, assuming, however, a harmonic primary excitation at each frequency line of interest. The reason for this definition is that an optimisation process at a single frequency produces optimal sensor and actuator locations which are different for different excitation frequencies (for example on-resonance and off-resonance). As the sensor and actuator configuration cannot be changed with the excitation frequency, the objective function definition should include the dynamic properties of the actively controlled system over the entire frequency band of interest. Therefore, the optimisation with respect to the broadband radiated sound power should result in a control system with a reasonable broadband performance and a good robustness against changes in the disturbing excitation frequency.

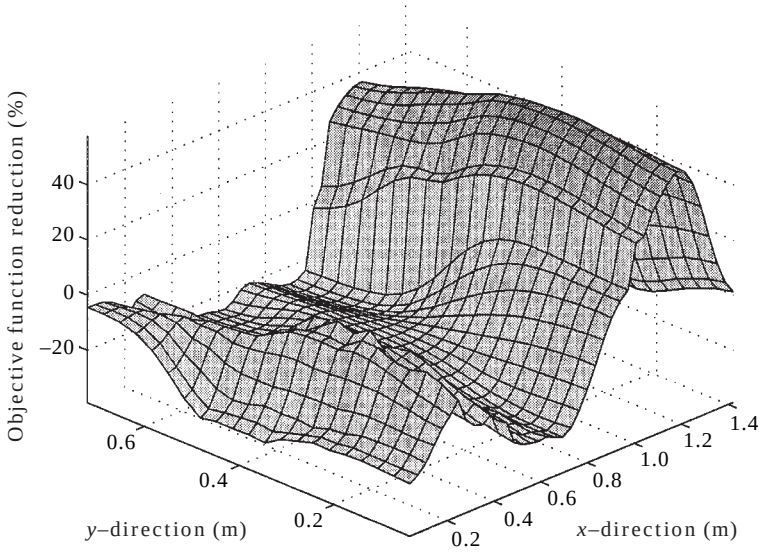

Figure 2. Reduction of the average radiated sound power as a function of the position of one control loudspeaker in the mid-plane of the trim cavity.

5. GENETIC ALGORITHMS

The objective function equation (22) has first been optimised by means of a genetic algorithm [13, 14]. Genetic algorithms belong to the so-called directed random search techniques. The form of direction is based on Darwin's "survival of the fittest" theories.

5.1. DESCRIPTION OF THE ALGORITHMS

For the present study, a genetic algorithm using a binary coding of the variables in the optimisation process has been used. The feasible positions for the control actuators and the error sensors are restricted to 4080 discrete positions equally distributed over the skin panel, the trim panel and the cavity between both panels. The positions coincide with those nodes of the FE model which are at least at 5 cm from the border of the vibro-acoustic structure (in order to allow also the practical implementation of the optimised configuration). Each position is coded in a 12-bit binary representation. One gene consists of the binary representations for the error sensor positions ("p_1" to "p_4") and the control actuator positions ("p_5" and "p_6") one after each other, augmented with four bits to activate the sensors ("e_1" to "e_4") and another two bits to activate the actuators ("c_1" and "c_2"):

$$\text{gene} = [e_1\ e_2\ e_3\ e_4 \mid c_1\ c_2 \mid p_1\ p_2\ p_3\ p_4\ p_5\ p_6]. \tag{26}$$

When optimising, for example, the positions for a control system with up to two control loudspeakers and up to four error microphones, one gene contains six activation bits and six binary coded locations of 12 bits each, resulting in 78 bits in total. Each gene is attributed a weighting based on the value of its *fitness*

function F, defined as the percentage reduction of the objective function, diminished with a penalty for each error sensor and each control actuator:

$$F = \frac{\Pi_0 - \Pi_c}{\Pi_0} * 100\% - (\#\ \text{sensors}) * a\% - (\#\ \text{actuators}) * b\%, \tag{27}$$

where the subscript o refers to the situation without active control and the subscript c to the situation with active control. The choice of the penalties a and b is based on a trade-off between the marginal yield, gained by a further decrease of the radiated sound power, and the extra cost incurred by adding one sensor or one actuator respectively to the control system. In the present study, the penalties a and b have been chosen arbitrarily as 0·25 and 0·5, respectively. With this definition for the objective function, it is possible to optimise not only the positions of the error sensors and the control actuators, but also their number (by means of the activation bits) and type. Depending on its position, a sensor can be either a microphone or an accelerometer, and an actuator can be either a loudspeaker or a shaker.

The big advantage of a genetic algorithm is the fact that it undertakes a wider search in the entire design variable space than the conventional descent algorithms. This is mainly due to the random character of the procreation process in the genetic operators. From past experiences [18], however, it is clear that this lack of descent information causes the algorithm to proceed only very slowly from one good point in the neighbourhood of the (possibly local) optimum to a better point (closer to the optimum). For this reason, an attempt has been made to incorporate some gradient-based behaviour in the genetic algorithm. Each time the genetic algorithm finds a new best gene, the fitness function is evaluated for all sensor and actuator configurations which are directly adjacent to the current configuration, the resulting fitness functions are ranked, and the best gene in the mating pool is replaced by the best adjacent configuration if the fitness function of this latter is better than that of the considered best gene. As the possible sensor and actuator locations coincide with nodes of the finite element model, the configurations adjacent to a considered configuration are found by means of the information in the finite element model.

It is nevertheless important to notice that this gradient-based behaviour does not replace the guided random search in the conventional genetic algorithm, it is only supplementary to this guided random search. The main characteristics of the genetic algorithm used in this study can be found in references [18, 32].

5.2. DISCUSSION OF THE ALGORITHM PERFORMANCES

Figure 3 shows the evolution of a completely random search process (dashed line), of the conventional genetic algorithm (solid line) and of the genetic algorithm with gradient-based behaviour (dash-dotted line) as a function of the number of floating point operations (flops). The initial mating pool contained 40 randomly generated genes. The crossover, mutation and translation probabilities have been selected as 0·8, 0·2 and 0·4, respectively, based on extensive previous trials [18, 32].

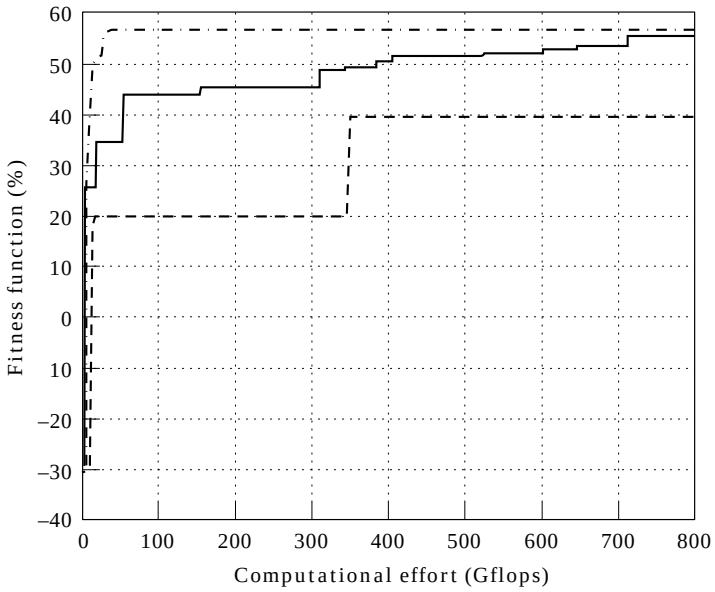

Figure 3. Evolution of the conventional genetic algorithm (solid line), of the genetic algorithm with gradient-based behaviour (dash-dotted line), and of a random search process (dashed line).

Figure 3 shows that the performance of both genetic algorithms largely exceeds that of the random search process. It also clearly indicates that the genetic algorithm with gradient-based behaviour (dash-dotted line) converges much quicker than the conventional algorithm (solid line). Already after less than one tenth of the total computation time, the new genetic algorithm reaches its final solution. This means that, in future applications, the optimisation process can be stopped much earlier than with the conventional genetic algorithm. Besides the fact that the convergence is much faster, the final solution is also somewhat better. The average population fitnesses of both genetic algorithms show a similar evolution, indicating that the genetic algorithm with gradient-based behaviour is not suffering from premature convergence. This proves that the random search component is only supplemented and not replaced by the gradient search component.

6. GRADIENT METHODS

This section investigates the use of some gradient algorithms as an alternative to the genetic algorithms, described in section 5. As already mentioned, conventional genetic algorithms suffer from the severe drawback that they require a huge amount of useless objective function evaluations due to the random character of the search process. The introduction of some gradient-based behaviour at certain iterations in the genetic algorithm increased dramatically the convergence speed of the genetic algorithm. A logical next step is then to explicitly use the gradient information in each iteration of the algorithm. Therefore, a mathematical expression for the gradient of the objective function (22) with respect to the sensor and actuator positions is derived in the

next section. In section 6.2, the classical non-linear optimisation algorithms, which are purely deterministic, are discussed. Afterwards, in section 6.3, the randomly perturbed gradient method [20–22] is applied to the considered problem.

6.1. ANALYTICAL COMPUTATION OF THE GRADIENT OF THE OBJECTIVE FUNCTION

The objective function defined in equation (22) is an implicit function of the sensor and the actuator positions:

$$\Pi = \Pi(\mathbf{r}_c, \mathbf{r}_e). \tag{28}$$

Considering a plane structure where the positions of the sensors and the actuators of the control system can only vary in the x- and the y-directions, the gradient of equation (28) is a vector of the following form:

$$[\nabla \Pi]^T = \left[\frac{\partial \Pi}{\partial x_1^c}\frac{\partial \Pi}{\partial y_1^c}\frac{\partial \Pi}{\partial x_2^c}\frac{\partial \Pi}{\partial y_2^c}\cdots\frac{\partial \Pi}{\partial x_c^c}\frac{\partial \Pi}{\partial y_c^c}\frac{\partial \Pi}{\partial x_1^e}\frac{\partial \Pi}{\partial y_1^e}\frac{\partial \Pi}{\partial x_2^e}\frac{\partial \Pi}{\partial y_2^e}\cdots\frac{\partial \Pi}{\partial x_e^e}\frac{\partial \Pi}{\partial y_e^e}\right]^T. \tag{29}$$

This vector contains $2x(c+e)$ elements, in which c is the number of control actuators and e is the number of error sensors. In a more general three-dimensional case, also the partial derivatives of the objective function with respect to the z co-ordinate of the positions of the sensors and the actuators should be taken into account. In the present study on the simplified aircraft fuselage test section model, the z-dependency is only relevant for the positions of acoustical sensors and actuators in the trim cavity, and is related to a variation of the positions in the thickness direction of the trim cavity. It is neglected here for sake of simplicity. The first element of the gradient (29) is the partial derivative of the objective function with respect to the x co-ordinate of the position of the first actuator. This derivative can be calculated using the definition of the objective function (22):

$$\frac{\partial \Pi}{\partial x_1^c} = \frac{1}{f_N - f_0}\sum_{f=f_0}^{f_N}\left(\frac{\partial\{\dot{\mathbf{u}}_{trim}\}^H}{\partial x_1^c}[\boldsymbol{\Sigma}]\{\dot{\mathbf{u}}_{trim}\} + \{\dot{\mathbf{u}}_{trim}\}^H[\boldsymbol{\Sigma}]\frac{\partial\{\dot{\mathbf{u}}_{trim}\}}{\partial x_1^c}\right). \tag{30}$$

The partial derivative of the trim panel velocity $\{\dot{\mathbf{u}}_{trim}\}$ with respect to the x co-ordinate of the position of the first actuator is obtained using equations (4) and (22):

$$\begin{aligned}\frac{\partial\{\dot{\mathbf{u}}_{trim}\}}{\partial x_1^c} = &-\mathrm{j}\omega[\boldsymbol{\Phi}_s]_{trim}[\mathbf{a}]^{-1}\frac{\partial[\bar{\boldsymbol{\Phi}}(\mathbf{r}_c)]^H}{\partial x_1^c}[\mathbf{h}]^+[\boldsymbol{\Phi}(\mathbf{r}_e)][\mathbf{a}]^{-1}[\bar{\boldsymbol{\Phi}}]^H\{\mathbf{F}\}_p \\ &-\mathrm{j}\omega[\boldsymbol{\Phi}_s]_{trim}[\mathbf{a}]^{-1}[\bar{\boldsymbol{\Phi}}(\mathbf{r}_c)]^H\frac{\partial[\mathbf{h}]^+}{\partial x_1^c}[\boldsymbol{\Phi}(\mathbf{r}_e)][\mathbf{a}]^{-1}[\bar{\boldsymbol{\Phi}}]^H\{\mathbf{F}\}_p.\end{aligned} \tag{31}$$

The partial derivative of the pseudo-inverse of the matrix $[\mathbf{h}]$ depends on the partial derivative of the matrix $[\mathbf{h}]$ itself and on its pseudo-inverse:

$$\frac{\partial[\mathbf{h}]^{+}}{\partial x_1^c} = -[\mathbf{h}]^{+}\frac{\partial[\mathbf{h}]}{\partial x_1^c}[\mathbf{h}]^{+} + [\mathbf{h}]^{+}([\mathbf{h}]^{+})^{H}\left(\frac{\partial[\mathbf{h}]}{\partial x_1^c}\right)^{H}([\mathbf{I}] - [\mathbf{h}][\mathbf{h}]^{+}). \tag{32}$$

The partial derivative of the matrix [**h**] with respect to the x co-ordinate of the position of the first actuator is easily obtained using equation (21):

$$\frac{\partial[\mathbf{h}]}{\partial x_1^c} = [\mathbf{\Phi}(\mathbf{r}_e)][\mathbf{a}]^{-1}\frac{\partial[\bar{\mathbf{\Phi}}(\mathbf{r}_c)]^{H}}{\partial x_1^c}. \tag{33}$$

It is important to notice here that both the [**a**] and the [**h**] matrices are frequency-dependent. As the entire partial derivative (30) of the objective function to the x co-ordinate of the position of the first actuator consists of a summation over all frequency lines, its calculation is very time-consuming, especially when a large number of sensors and actuators are used. In this case the matrix [**h**] (dimension *exc*) becomes large and the computation of the partial derivative of the pseudo-inverse of the matrix [**h**] (32) becomes practically infeasible. However, for a small number of sensors and actuators, the computationally most demanding step in the gradient evaluation is the calculation of the sensitivity of the mode shapes for the actuator x co-ordinate (appearing in equations (31) and (33)) by means of finite differences. This calculation is based on two-dimensional interpolations in the mode shape matrix [**Φ**], which is only "exactly" known in the nodes of the finite element model. As this mode shape matrix [**Φ**] is not frequency-dependent, the calculation of all sensitivities of the mode shapes for all actuator and sensor co-ordinates can be performed beforehand. This reduces the total calculation time for one gradient evaluation to about three to four times the calculation time for one function evaluation for the case of an active control system with two control actuators and four error sensors. The expression for the partial derivatives, which is derived in terms of Cartesian co-ordinates in the present case of a rectangular geometry, can also be written in terms of a different parameterisation in the case of curved two- or three-dimensional geometries.

The equations needed for the calculation of the other partial derivatives of the objective function to one of the control actuator or error sensor co-ordinates are derived in a similar way.

6.2. COMPARISON OF THE DIFFERENT NON-LINEAR OPTIMISATION METHODS

Four gradient-based methods [33–35] have been implemented (the Fletcher–Reeves method, the Polak–Ribière method, the BFGS (Broyden–Fletcher–Goldfarb–Shanno) quasi-Newton method and the Han–Powell method). Basically the Han–Powell method uses a sequential quadratic programming algorithm, and was originally developed for solving constrained optimisation problems. Obviously no constraints are present in the considered problem, but the design variables are nevertheless bounded within positions on the edges of the test structure. The Fletcher–Reeves, the Polak–Ribière and the BFGS

method are methods for solving unconstrained optimisation problems. The basic structure of any unconstrained gradient-based method is as follows:

Start at an initial point x_0

Iteration k

1. *Calculate* $f_k = \Pi(x_k)$
   $g_k = grad(\Pi(x_k))$
   $H_k = Hessian(\Pi(x_k))$ *(if necessary)*
   Test optimality
2. *Choose a search direction* $d_k \neq 0$
3. *Perform a line-search* : $x_{k+1} = x_k + \alpha_k d_k$
   with $\alpha_{k+1} = arg\ min\ \Pi(x_k + \alpha d_k)$, *and* $\alpha_k > 0$

End

The search direction d_k is determined as follows for $k>0$: for the Fletcher–Reeves method:

$$d_k = -g_k + \frac{\| g_k \|^2}{\| g_{k-1} \|^2} d_{k-1}, \tag{34}$$

for the Polak–Ribière method:

$$d_k = -g_k + \frac{g_k^T (g_k - g_{k-1})}{\| g_{k-1} \|^2} d_{k-1}, \tag{35}$$

and for the BFGS method:

$$d_k = B_k^{-1}(-g_k), \tag{36}$$

where the approximated Hessian B_k is calculated as:

$$B_{k+1} = B_k - \frac{B_k p_k p_k^T B_k}{p_k^T B_k q_k} + \frac{q_k q_k^T}{p_k^T q_k}, \text{ with } p_k = x_{k+1} - x_k \text{ and } q_k = g_{k+1} - g_k. \tag{37}$$

The initial search direction is the same for all algorithms:

$$d_0 = -g_0. \tag{38}$$

Two different approaches for imposing bounds on the design variables have been tested in this study. The first method consists of introducing penalty functions, which artificially penalise the objective function when one of the design variables approaches one of the bounds. In the second method, the bounds are immediately taken into account in the line-search procedure. Before starting the iteration on the line-search variable α, its maximum value α_{max} is determined such that a step of size α_{max} along the direction d_k never produces a new point x_{k+1} whose components exceed their upper or lower bounds. A one-dimensional minimisation algorithm is then used to solve the following problem:

$$\min_{0 \le \alpha \le \alpha_{max}} \varphi(\alpha), \quad \text{with } \varphi(\alpha) = \Pi(x_k + \alpha d_k). \tag{39}$$

It first tries to find a value α_u for α such that:

$$\varphi(\alpha_u) \ge \varphi(0). \tag{40}$$

Moreover, when the search direction is a descent direction, the following holds:

$$\varphi'(0) = g_k^T d_k \le 0. \tag{41}$$

When equations (40) and (41) are satisfied, a (local) minimum of $\varphi(\alpha)$ is trapped between 0 and α_u. Quadratic and cubic interpolation procedures are then used to successively generate improved estimates of the solution of the one-dimensional minimisation problem (39).

In order to allow an objective comparison between the different non-linear optimisation methods, each method has been tested on the *same* set of 25 samples of randomly generated initial positions for two control actuators on the skin panel and four error sensors on the trim panel. Due to the relatively high modal density of the aircraft fuselage test section, the control system achieves a reduction of the radiated sound power, compared to the situation without active control, only in 4 out of the 25 initial configurations. This illustrates the need for a good optimisation algorithm to improve the performance of the active control system.

The set of 25 samples is submitted to each method, once with and once without the supply of analytical gradients. In the latter case the algorithms estimate the gradient of the objective function augmented with penalty functions in each iteration step using a finite difference approximation. Two versions of the Fletcher–Reeves, the Polak–Ribière and the BFGS methods with analytical gradients have been tested, the first with the penalty functions and the second with the bounded line-search procedure. In order to limit the total computation time, each method is terminated after only 50 iterations. This number is relatively small compared to the number of design variables, which is 12, being the x- and y-positions for the four error sensors and the two control actuators. Figure 4 shows the percentage reduction in the objective function for the optimised control configurations of the samples using the BFGS quasi-Newton method. The bars in the dashed line give the results obtained using the analytically supplied gradients and the penalty functions, the bars in the dotted line give the results using the analytically supplied gradients and the bounded line-search procedure, while the bars in the solid line give the results when the gradients are approximated with finite differences. Figures 5 and 6 show the same results for the Polak–Ribière and the Fletcher–Reeves methods, respectively. Figure 7 gives the results for the Han–Powell method. The bars in the dashed line correspond to the case with analytical gradients and the bars in the solid line to the case with finite differences.

A visual comparison between these figures gives already an indication of the quality of the different methods for the optimisation of the sensor and actuator

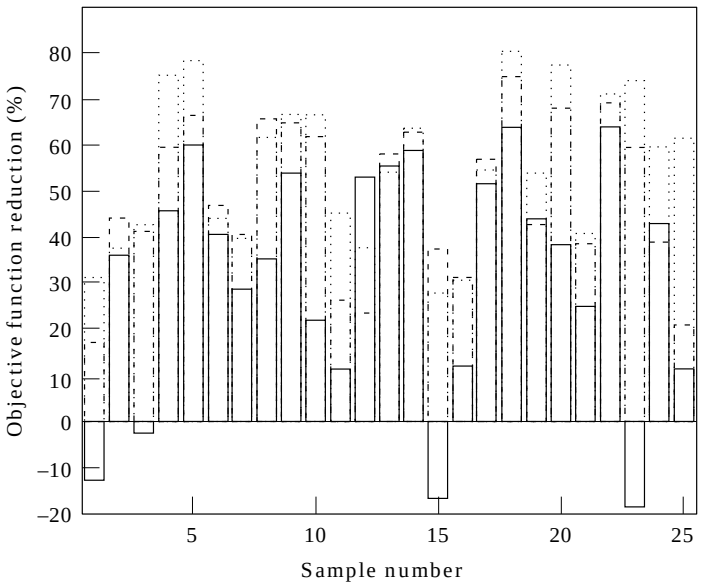

Figure 4. Percentage reduction in the objective function for the optimised control configurations of the samples using the BFGS method, with analytical gradients and penalty functions (dashed line), with analytical gradients and the bounded line-search procedure (dotted line), and with finite differences (solid line).

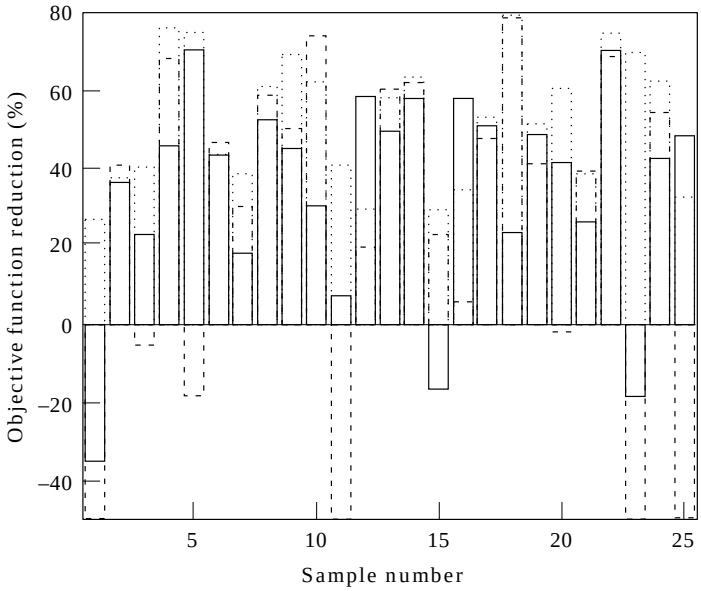

Figure 5. Percentage reduction in the objective function for the optimised control configurations of the samples using the Polak–Ribière method, with analytical gradients and penalty functions (dashed line), with analytical gradients and the bounded line-search procedure (dotted line), and with finite differences (solid line).

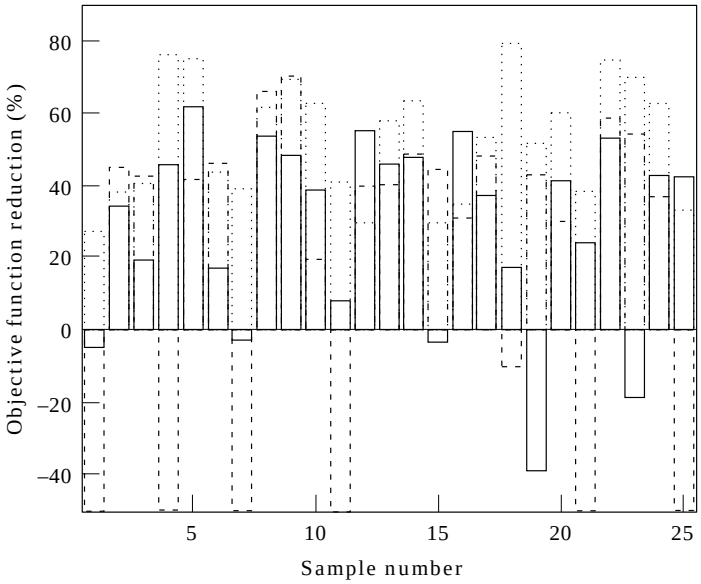

Figure 6. Percentage reduction in the objective function for the optimised control configurations of the samples using the Fletcher–Reeves method, with analytical gradients and penalty functions (dashed line), with analytical gradients and the bounded line-search procedure (dotted line), and with finite differences (solid line).

positions in an active control system. However, a more founded statistical treatment of the test results is necessary to infer reliable conclusions about the relative performances of the methods. As the test results are not normally distributed, the classical methods for hypothesis testing and analysis of variance, which assume a normal distribution for the test statistic, are not applicable. Therefore, the Wilcoxon signed ranks test [36, 37], which is a non-parametric test, is used here. Non-parametric tests do not make any particular assumptions about the probability distributions of the test statistic. As all methods are tested on the same set of samples, a statistical test for paired samples is used, because it provides much more statistical information than a test for two sets of independently generated samples of the same size.

The Wilcoxon signed ranks test detects shifts in locations of population relative frequency distributions for data collected as paired samples. To perform the test, ranks are assigned to the absolute values of the differences. Differences equal to zero are eliminated and the number n of differences is reduced accordingly. Let now D_1 and D_2 represent the population relative frequency distributions for populations 1 and 2, respectively. The null hypothesis H_0 is "D_1 and D_2 are identical", and, for a one-sided test, the alternative hypothesis H_a is "D_1 is shifted to the right of D_2". The test statistic is T^-, the rank sum of the negative differences, and the rejection region is:

$$T^- \leq T_0, \tag{42}$$

where T_0 is given in a table with critical values for the Wilcoxon signed ranks test for different levels of significance [37]. This means that, if equation (42) is

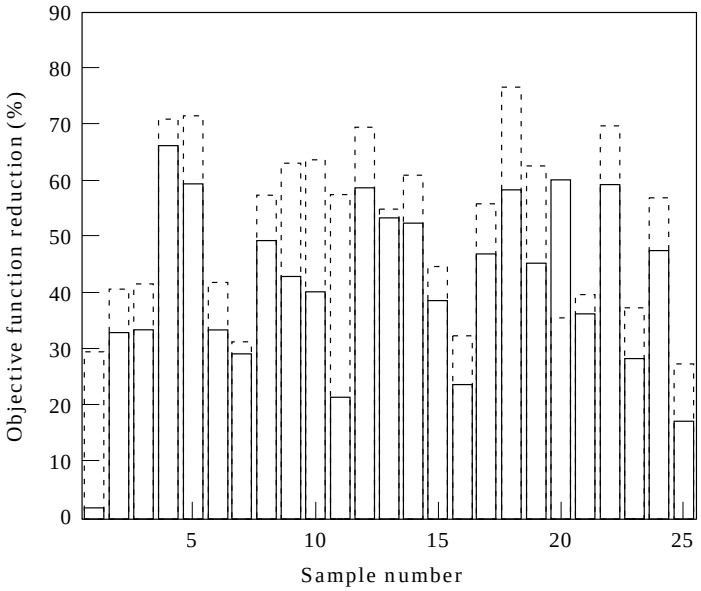

Figure 7. Percentage reduction in the objective function for the optimised control configurations of the samples using the Han–Powell method, with analytical gradients (dashed line), and with finite differences (solid line).

satisfied, the null hypothesis can be rejected with sufficient statistical significance, and hence there really is a difference between the means of the two populations.

First the Wilcoxon test is used to determine whether the use of analytically supplied gradients significantly improves the convergence behaviour of the gradient-based methods. For this test the results of all gradient methods are pooled in two sets, the first for the calculations with analytical gradients and penalty functions and the second for calculations with finite difference approximations. The null hypothesis H_0 states that the means of both sets are equal, while the alternative hypothesis H_a states that the mean of the first set is larger than that of the second set. Based on the Wilcoxon test, the null hypothesis H_0 is rejected with a significance level of 1%. Although the gradient computations are also based on interpolations for estimating the modal amplitudes ($[\bar{\mathbf{\Phi}}(\mathbf{r_c})]$ and $[\mathbf{\Phi}(\mathbf{r}_e)]$) and their derivatives (for example $\partial[\bar{\mathbf{\Phi}}(\mathbf{r}_c)]/\partial x_1^c$) between the nodes of the finite element model, this test shows that the convergence behaviour of the non-linear optimisation algorithms improves when gradient information is provided from analytical calculations using equations (29) to (33). This result suggests that, due to the additional information, which is supplied by the analytical expressions, the explicit gradient evaluation drastically reduces the interpolation error in comparison with the finite difference approximations of the objective function, which estimate directly $\partial \Pi/\partial x_1^c$ and the other partial derivatives in equation (29). This result clearly appears in the Figures 4 and 7 by comparing the bars in the solid line with the two other types, but may be less obvious in Figures 5 and 6.

Second, the Wilcoxon signed ranks test also indicates with a significance level of 1% that, when using the unconstrained optimisation routines (Fletcher–

Reeves, Polak–Ribière or BFGS), the bounded line-search procedure, which has been developed in this study, yields much better results than a conventional unbounded line-search procedure combined with penalty functions. As these penalty functions have very large gradients close to the bounds on the variables, they can completely dominate the gradient of the total objective function (with the penalty functions included), and hence push the search process in the wrong direction. For this reason, the incorporation of the new bounded line-search procedure in the BFGS, the Polak–Ribière and the Fletcher–Reeves methods, allowing the solution of bounded unconstrained optimisation problems, dramatically improves the performances of these methods. This conclusion is clearly illustrated in Figures 4 to 6 by a comparison of the bars in the dashed line (i.e., with penalty functions) with the bars in the dotted line (i.e., with the bounded line-search procedure).

Finally, the performances of the different optimisation methods are also compared using the Wilcoxon signed ranks test with a significance level of 5%. The populations consist of the results of the experiments both with analytically supplied gradients and with finite differences, as this increases the power of the statistical test. The Wilcoxon test indicates that the BFGS and the Polak–Ribière methods are superior to the Fletcher–Reeves method. It also shows that the Han–Powell method, which uses a complex sequential quadratic programming algorithm, does not outperform the best unconstrained gradient-based optimisation methods (BFGS and Polak–Ribière). Especially when they use the bounded line-search procedure and analytically calculated gradients (the dotted bars in Figures 4 and 5), they perform at least as well as the Han–Powell method. Moreover, because of their simplicity the unconstrained algorithms can be adapted much more easily to possible peculiarities of the problem that has to be solved, and are therefore preferable for the present application.

6.3. THE RANDOMLY PERTURBED GRADIENT METHOD

The previous section showed that many of the classical non-linear optimisation methods perform well when started from some randomly generated set of initial sensor and actuator positions. One major drawback of these methods is their convergence to a possible local optimum. The introduction of some random search component may increase the probability of converging to the global optimum. Therefore, Pogu and Souza de Cursi [21] suggested applying a random perturbations on the steepest descent method with a fixed step size. They theoretically proved that their algorithm generates a bounded minimising sequence, leading to the global optimum [21, 22]. The structure of their algorithm is similar to that presented in section 6.2, except for the line-search step that is replaced by:

3.*a Generate n random vectors* Z_i *inside the search domain.*
3.*b Set* $Z_0=\{0\}$, *and* $x_{k+1} = argmin_{0<i<n}\, \Pi(x_k+\alpha d_k+\lambda_k Z_i)$.

According to references [20–22], the step size α is fixed, as opposed to the algorithm of section 6.2 where it is the result of a one-dimensional minimisation process along the search direction.

The sequence $\{\lambda_k\}_{k\leqslant 0}$ decreases monotonically for increasing iteration number k:

$$\lambda_k = \sqrt{\frac{c}{\log(k+d)}}. \tag{43}$$

When the theoretical restrictions on the constants c and d of references [21, 22] are respected, it satisfies the following inequality:

$$\forall k \geq 0 : 0 < \lambda_k < 1 - \sqrt{1-\varepsilon}, \tag{44}$$

with ε a small positive real number. However, these theoretical restrictions are difficult to validate in practice, and the corresponding theoretical values for λ_k are pessimistic, as indicated by Pogu and Souza de Cursi [21]. For that reason, the values of c and d have been set to unity, similarly as in references [20–22]. The number of random vectors n used in each iteration greatly determines the number of objective function evaluations in the optimisation process. In order to limit the computation time per iteration, five random vectors are used in step 3.b of the algorithm. Moreover, the average number of function evaluations in the line-search step in the algorithm of section 6.2 appears also to be five.

Figure 8 shows the evolution of the algorithm for different values of the step size α (dashed line: 0·01, solid line: 0·02, dash-dotted line: 0·05, and dotted line: 0·1). As the objective function does not have a smooth behaviour, large step sizes yield an oscillating search process dominated by the random search component. For small step sizes, the algorithm moves very slowly through the valleys in the objective function, and the random perturbations have no influence. As a compromise, a step size of 0·02 has been selected for all subsequent calculations with the randomly perturbed gradient method.

The same set of 25 initial sensor and actuator positions as in section 6.2 has been used here to investigate the influence of the type of search direction d_k. This analysis shows that the quasi-Newton (BFGS) and the Polak–Ribière methods do not improve the convergence behaviour of the algorithm in comparison with the steepest descent method that was proposed by Pogu and Souza de Cursi [21]. The Wilcoxon test also shows, with a significance level of 1%, that the randomly perturbed gradient method with analytically calculated gradients yields much better results than that using finite difference approximations of the gradient.

7. COMPARISON BETWEEN THE GENETIC ALGORITHMS AND THE GRADIENT METHODS

Four different types of optimisation algorithms have been tested in this study: the genetic algorithm, the genetic algorithm with gradient-based behaviour, the randomly perturbed gradient methods, and the classical deterministic gradient methods. The discussion on the genetic algorithms in section 5.2 clearly shows that the performance of the genetic algorithms is drastically improved by supplementing the directed random search, which is characteristic for the genetic algorithm, with some gradient search. In this case, the random search

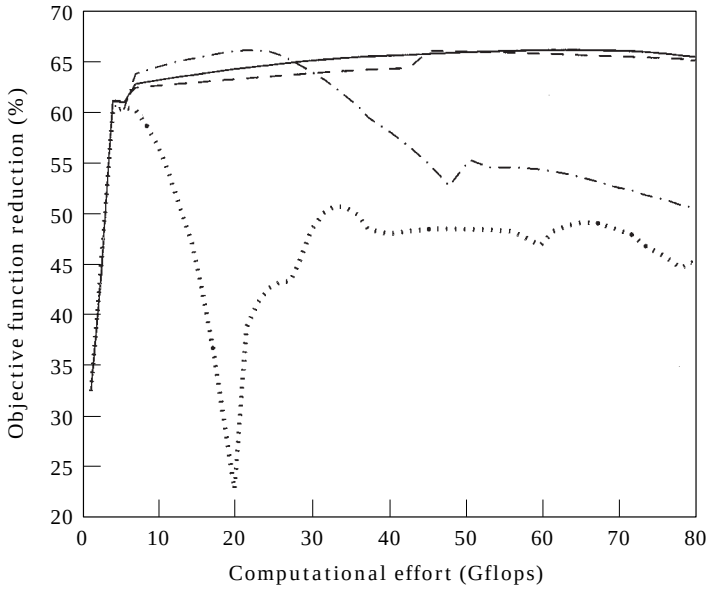

Figure 8. Evolution of the randomly perturbed gradient method with a step size of 0·01 (dashed line), 0·02 (solid line), 0·05 (dash-dotted line), and 0·1 (dotted line).

component aims at exploring the entire search domain, while the gradient search component speeds up the local convergence to the optimum.

A similar motivation led Pogu and Souza de Cursi [21] to the extension of the classical deterministic steepest descent method with a random search component. The main disadvantage of their method is the fixed step α along the deterministic search direction. Due to this fixed step, the algorithm does not achieve a guaranteed improvement in the objective from one iteration to the next. To illustrate this, Figure 9 shows the evolution of the randomly perturbed gradient method with step size 0·01 (dashed line), 0·02 (dash-dotted line) and 0·05 (dotted line) and of the BFGS quasi-Newton method (in solid line). The BFGS method achieves in each iteration a minimal decrease in the radiated sound power, but this is not the case for the randomly perturbed gradient methods. Figure 10 shows the results of the optimisation on the same set of 25 initial positions for the BFGS and the randomly perturbed gradient method. A formal comparison of these results using the Wilcoxon signed rank test indicates with a significance level of more than 1% that the BFGS method is superior to the randomly perturbed steepest descent method.

As shown in Figure 3, the genetic algorithm with gradient-based behaviour (dash-dotted line) finds a good sensor and actuator configuration, which reduces the fitness function by almost 57%, after almost 50 billion floating point operations. Referring to the definition of the fitness (27), this corresponds to an average reduction of the radiated sound power between 20 and 250 Hz of almost 59% (or 3·9 dB) for a system with four error sensors and two control actuators. When the BFGS method uses this solution as a starting point, it produces after another 50 billion flops a solution that reduces the average radiated sound power by 81% (7·2 dB). This strongly contrasts with the dash-dotted curve in Figure 3,

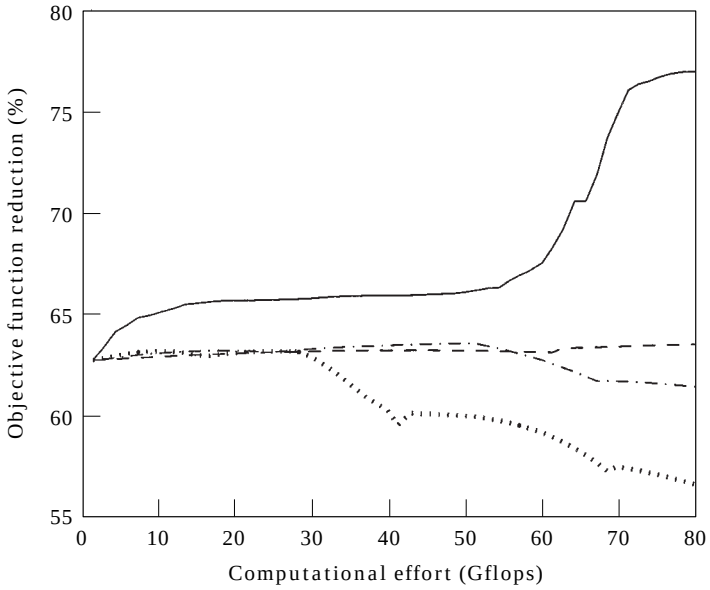

Figure 9. Evolution of the BFGS method (solid line) and of the randomly perturbed gradient method with different step sizes (0·01: dashed line, 0·02: dash-dotted line, and 0·05: dotted line).

where the genetic algorithm does not yield any improvement in the best solution after more than 800 billion floating point operations.

The BFGS algorithm with analytically supplied gradients, has been tested with a starting point, corresponding to the best configuration out of 50 randomly

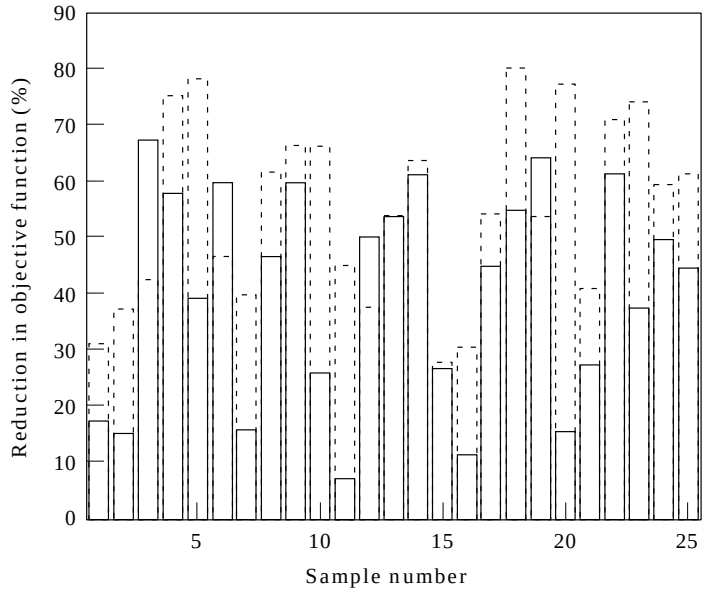

Figure 10. Percentage reduction in the objective function for the optimised control configurations of the samples using the BFGS method (dashed line), and the randomly perturbed steepest descent method (solid line).

generated configurations. The control system with sensors and actuators in this starting configuration reduces the average radiated sound power by 32% (1·7 dB). After a similar number of floating point operations (50 billion) the BFGS algorithm produces a sensor and actuator configuration which reduces the trim panel vibration energy by 73% (5·7 dB).

These experiments indicate that the best strategy for optimising the sensor and actuator locations in an active control system is to use a classical non-linear optimisation method, if possible with analytically calculated gradients, and to allow multiple runs starting from different initial configurations (the so-called multi-start procedure). These initial configurations can be selected with some engineering judgement or at random. Alternatively, a single, good starting configuration can be selected out of the objective function evaluations on some sets of randomly generated configurations.

The experiments also show that the genetic algorithms, which were recently introduced for optimising the sensor and actuator positions in an active control system, are not superior to the good gradient methods. In the present case, the non-linear method even produces a better solution than the genetic algorithm in a similar amount of computation time. This finding agrees with the comment by Pogu and Souza de Cursi [21] who consider genetic algorithms and other random search techniques only as "last resort" methods for solving continuous optimisation problems. However, the big advantage of the genetic algorithm is that it is inherently well suited for solving discrete optimisation problems, arising, for example, in the sensor and actuator location optimisation on experimentally determined models in a very coarse grid of the search domain under study. Moreover, the genetic algorithm, as presented here, allows one to optimise both the number and the locations of the actuators and the sensors, and its implementation is quite simple.

8. CONCLUSIONS

The optimisation of the positions of the sensors and the actuators in an active noise control system has been studied. This active control system is implemented on a double panel partition, representing a section of an aircraft fuselage, and aims at increasing the sound transmission loss in the low-frequency range. The control actuators can be either loudspeakers in the cavity, or shakers on the panels, and the error sensors can be either microphones in the cavity, or accelerometers on the panels. The sound transmission loss of the actively controlled double panel partition strongly depends on the locations of the sensors and the actuators. This optimisation study uses an integrated simulation model that is based on an experimentally validated vibro-acoustic FE model of the double wall structure and on a simplified model of the control system. This integrated simulation model describes the dynamic behaviour of the actively controlled double panel partition. The acoustic power, radiated by the trim panel in the frequency band of interest, is the objective function in the optimisation process.

This objective function has first been optimised by means of a genetic algorithm. Two variants of the usual genetic algorithm have been proposed and tested on the considered problem. It appears that the incorporation of some gradient-based behaviour in the genetic algorithm can significantly increase its convergence speed, without eliminating the advantage of the guided random search process. The big advantage of the genetic algorithm is that it is inherently well-suited for solving discrete optimisation problems and that its implementation is quite simple.

Also a number of classical non-linear optimisation algorithms have been implemented for solving the considered optimisation problem. These methods have been tested on a set of starting points, as well with analytically calculated gradients as with gradients approximated by finite differences. The Wilcoxon signed ranks test indicates that the use of analytically supplied gradients significantly improves the performance of the algorithms, and that the bounds on the design variables should be introduced in the line-search procedure, and not by using penalty functions. The simple Polak–Ribière and BFGS methods perform at least as well as the complex Han–Powell method in the considered optimisation problem.

The randomly perturbed gradient method by Souza de Cursi, that tries to combine the good local convergence characteristics of the gradient methods with the global optimisation capabilities of the random search techniques, does not yield very good results for the problem being considered here. Its main drawbacks are the fixed step size, and the difficult selection of the tuning parameters.

The main conclusion of this study is that the simple unconstrained gradient methods, with a bounded line-search and analytically calculated gradients, perform better than the genetic algorithms and the randomly perturbed gradient methods. The use of a limited number of different starting points extends these methods with some random search components in order to improve their global search capabilities.

ACKNOWLEDGMENT

This text presents research results of the Belgian Program on Interuniversity Poles of Attraction by the Belgian State, Prime Minister's Office, Science Policy Programming. The scientific responsibility is assumed by the authors.

The first author is Research Assistant of the Fund for Scientific Research-Flanders (Belgium) (F.W.O.).

REFERENCES

1. R. L. CLARK and C. R. FULLER 1992 *Journal of the Acoustical Society of America* **92**, 1521–1533. Optimal placement of piezoelectric actuators and polyvinylidene fluoride sensors in active structural acoustic control approaches.
2. B.-T. WANG, R. A. BURDISSO and C. R. FULLER 1994 *Journal of Intelligent Material Systems and Structures* **5**, 67–77. Optimal placement of piezoelectric actuators for active structural acoustic control.

3. T. C. YANG, C. H. TSENG and S. F. LING 1994 *Journal of the Acoustical Society of America* **95**, 3390–3399. Constrained optimisation of active noise control systems in enclosures.
4. P. H. NELSON and S. J. ELLIOT 1992 *Active Control of Sound*. London: Academic Press.
5. B. NAYROLES, G. TOUZOT and P. VILLON 1994 *Journal of Sound and Vibration* **171**, 1–21. Using diffuse approximation for optimising the location of anti-sound sources.
6. E. BENZARIA and V. MARTIN 1995 *Proceedings of Active* 95, 499–510. Constrained optimisation of secondary source locations : multipolar source arrangements.
7. E. BENZARIA and V. MARTIN 1994 *Journal of Sound and Vibration* **173**, 137–144. Secondary source locations in active noise control: selection or optimisation?
8. R. A. BURDISSO and C. R. FULLER 1992 *Journal of Sound and Vibration* **153**, 437–451. Theory of feedforward controlled system eigenproperties.
9. R. A. BURDISSO and C. R. FULLER 1992 *Journal of the Acoustical Society of America* **92**, 277–286. Dynamic behaviour of structural–acoustic systems in feedforward control of sound radiation.
10. R. A. BURDISSO and C. R. FULLER 1994 *AIAA Journal of Guidance, Control and Dynamics* **17**, 466–472. Feedforward controller design by eigenvalue assignment.
11. H. M. RODRIGUEZ, R. A. BURDISSO and C. R. FULLER 1994 *Proceedings of Active* 95, 335–346. Optimum design for feedforward active structural acoustic control of complex structures.
12. R. A. BURDISSO and C. R. FULLER 1994 *Journal of the Acoustical Society of America* **96**, 1582–1591. Design of active structural acoustic control systems by eigenproperty assignment.
13. D. E. GOLDBERG 1989 *Genetic Algorithms in Search, Optimisation and Machine Learning*. New York: Addison-Wesley.
14. K. S. TANG, K. F. MAN, S. KWONG and Q. HE 1996 *IEEE Signal Processing Magazine* Nov. 96. Genetic algorithms and their applications.
15. D. T. TSAHALIS, S. K. KATSIKAS and D. A. MANOLAS 1993 *Proceedings of Inter-Noise 93* **I**, 83–88. A genetic algorithm for optimal positioning of actuators in active noise control: results from the ASANCA project.
16. B.-T. WANG 1996 *Journal of the Acoustical Society of America* **99**, 2975–2984. Optimal placement of microphones and piezoelectric transducer actuators for far-field sound radiation control.
17. C. H. HANSEN, M. T. SIMPSON and C. T. WANGLER 1996 *Proceedings of the Fourth International Congress on Sound and Vibration* **I**, 371–388. Application of genetic algorithms to active noise and vibration control.
18. P. DE FONSECA, W. DEHANDSCHUTTER, P. SAS and H. VAN BRUSSEL 1996 *Proceedings of ISMA* 21, *Conference on Noise and Vibration Engineering* **I**, 377–388. Implementation of an active noise control system in a double glazing window.
19. K. H. BAEK and S. J. ELLIOT 1995 *Journal of Sound and Vibration* **186**, 245–267. Natural algorithms for choosing source locations in active control systems.
20. J. E. SOUZA DE CURSI and M. B. S. CORTES 1995 *Developments in Neural Networks and Evolutionary Computing for Civil and Structural Engineering*. Edinburgh: Civil-Comp Press. See pp. 189–198. General genetic algorithms and simulated annealing perturbation of the gradient method with a fixed parameter.
21. M. POGU and J. E. SOUZA DE CURSI 1994 *Journal of Global Optimization* **5**, 159–180. Global optimization by random perturbation of the gradient method wiht a fixed parameter.
22. L. AUTRIQUE and J. E. SOUZA DE CURSI 1997 *International Journal on Control* **76**, 1–21. On stochastic modification for global optimization problems: an efficient implementation for the control of the vulcanization process.

23. K. WYCKAERT, F. AUGUSZTINOVICZ and P. SAS 1996 *Journal of the Acoustical Society of America* **100**, 3172–3181. Vibro-acoustical modal analysis: reciprocity, model symmetry and model validity.
24. Z.-D. MA and I. HAGIWARA 1991 *American Institute of Aeronautics and Astronautic Journal* **29**, 1787–1795. Sensitivity analysis methods for coupled acoustic-structural systems, part I: modal sensitivities.
25. P. A. NELSON, A. R. D. CURTIS, S. J. ELLIOT and A. J. BULLMORE 1987 *Journal of Sound and Vibration* **117**, 1–13. The active minimisation of harmonic enclosed sound fields, part I: theory.
26. A. J. BULLMORE, P. A. NELSON, A. R. D. CURTIS and S. J. ELLIOT 1987 *Journal of Sound and Vibration* **117**, 15–33. The active minimisation of harmonic enclosed sound fields, part II: a computer simulation.
27. S. J. ELLIOT, A. R. D. CURTIS, A. J. BULLMORE and P. A. NELSON 1987 *Journal of Sound and Vibration* **117**, 35–58. The active minimisation of harmonic enclosed sound fields, part III: experimental verification.
28. S. D. SNYDER and C. H. HANSEN 1994 *Journal of Sound and Vibration* **170**, 433–449. The design of systems to control actively periodic sound transmission into enclosed spaces, part I: analytical models.
29. S. D. SNYDER and C. H. HANSEN 1994 *Journal of Sound and Vibration* **170**, 451–472. The design of systems to control actively periodic sound transmission into enclosed spaces, part II: mechanisms and trends.
30. P. VITIELLO, P. A. NELSON and M. PETYT 1989 *ISVR Technical Report* **183**. Numerical studies of the active control of sound transmissions through double partitions.
31. S. J. ELLIOT and M. E. JOHNSON 1993 *Journal of the Acoustical Society of America* **94**, 2194–2204. Radiation modes and the active control of sound power.
32. P. DE FONSECA, P. SAS and H. VAN BRUSSEL 1997 *Proceedings of SPIE's* 4*th Symposium on Smart Structures and Materials*, **3041**, 124–135. Optimization methods for choosing sensor and actuator locations in an actively controlled double panel partition.
33. S. S. RAO 1996 *Engineering Optimisation—Theory and Practice*. New York: Wiley; third edition.
34. P. BROUSSE 1988 *Optimisation in Mechanics: Problems and Methods*. Amsterdam: North-Holland series in Applied Mathematics and Mechanics, Elsevier Science Publishers B.V.
35. A. GRACE 1994 *Matlab Optimisation toolbox, User's guide*. The Mathworks Inc.
36. I. MILLER and J. E. FREUND 1985 *Probability and Statistics for Engineers*. Englewood Cliffs, NJ: Prentice-Hall; third edition.
37. T. SINCICH 1994 *A Course in Modern Business Statistics*. New York: Macmillan College Publishing Company.